Lab on a Chip

PAPER

View Article Online
View Journal | View Issue

Cite this: *Lab Chip*, 2019, **19**, 2362

3D-printing enabled micro-assembly of a microfluidic electroporation system for 3D tissue engineering†

Qingfu Zhu,[a] Megan Hamilton,[a] Bryan Vasquez[a] and Mei He *[ab]

Electro-transfection is an essential workhorse tool for regulating cellular responses and engineering cellular materials in tissue engineering. However, most of the existing approaches are only focused on cell suspensions *in vitro*, which fails to mimic an *in vivo* tissue microenvironment regarding the 3D electric field distribution and mass transport in a biological matrix. However, building a 3D electro-transfection system that is compatible with 3D cell culture for mimicking the *in vivo* tissue microenvironment is challenging, due to the substantial difficulties in control of the 3D electric field distribution as well as the cellular growth. To address such challenges, we introduce a novel 3D micro-assembly strategy assisted by 3D printing, which enables the molding of 3D microstructures as LEGO® parts from 3D-printed molds. The molded PDMS LEGO® bricks are then assembled into a 3D-cell culture chamber interconnected with vertical and horizontal perfusion microchannels as a 3D channel network. Such a 3D perfusion microchannel network is unattainable by direct 3D printing or other microfabrication approaches, which can facilitate the highly-efficient exchange of nutrition and waste for 3D cell growth. Four flat electrodes are mounted into the 3D culture chamber *via* a 3D-printed holder and controlled by a programmable power sequencer for multi-directional electric frequency scanning (3D μ-electro-transfection). This multi-directional scanning not only can create transient pores all over the cell membrane, but also can generate local oscillation for enhancing mass transport and improving cell transfection efficiency. As a proof-of-concept, we electro-delivered the pAcGFP1-C1 vector to 3D cultured HeLa cells within peptide hydrogel scaffolding. The expressed GFP level from transfected HeLa cells reflects the transfection efficiency. We found two key parameters including electric field strength and plasmid concentration playing more important roles than the pulse duration and duty cycles. The results showed an effective transfection efficiency of ~15% with ~85% cell viability, which is 3-fold higher compared to that of the conventional benchtop 3D cell electro-transfection. This 3D μ-electrotransfection system was further used for genetically editing 3D-cultured Hek-293 cells *via* direct delivery of CRISPR/Cas9 plasmid which showed successful transfection with GFP expressed in the cytoplasm as the reporter. The 3D-printing enabled micro-assembly allows facile creation of a novel 3D culture system for electro-transfection, which can be employed for versatile gene delivery and cellular engineering, as well as building *in vivo* like tissue models for fundamentally studying cellular regulation mechanisms at the molecular level.

Received 12th January 2019,
Accepted 6th June 2019

DOI: 10.1039/c9lc00046a

rsc.li/loc

Introduction

Intracellular delivery of regulatory or therapeutic targets into the cell is crucial for pharmacology studies as well as tissue engineering and regenerative medicine.[1,2] Among various delivery approaches such as using chemicals, ultrasound, and microneedles, electro-transfection has gained increasing popularity, due to its safe (free of harmful chemicals) and effective transfection, and no restrictions on cell types.[3–5]

Electro-transfection is also termed as electroporation, which gives rise to the transient permeabilization of the plasma membrane with temporary pores, due to the high local transmembrane potential induced by an external electric field. However, existing electro-transfection systems, including microfluidic platforms and commercial benchtop systems, are only able to study monolayer cell suspensions *in vitro*, and are incapable of clinical translation within an *in vivo* tissue microenvironment.[6–13] It has been well documented that cells growing in a two-dimensional (2D) culture

[a] *Department of Chemical and Petroleum Engineering, Bioengineering Program, University of Kansas, Lawrence, Kansas, USA. E-mail: meih@ku.edu*
[b] *Department of Chemistry, University of Kansas, Lawrence, Kansas, USA*

† Electronic supplementary information (ESI) available: Multi-directional frequency scanning video, as well as the monitoring of 3D cultured cells. See DOI: 10.1039/c9lc00046a

system significantly differ from living three-dimensional (3D) tissues in terms of cell morphology, functions, cell-to-cell communications, and cell-to-matrix adhesions.[14,15] Therefore, it is critical to use 3D cultured cells to represent an *in vivo*-like tissue microenvironment. The knowledge regarding the 3D electric field distribution and mass transport in a tissue microenvironment is lacking. Electroporation performed on cell suspensions is very often of limited use in 3D cells within a tissue microenvironment, because of the significant variations in terms of the membrane interactions, surrounding medium, extracellular matrix, orientation of cells to the electric fields and so on.[16,17] Thus, the clinical *in vivo* gene delivery faces tremendous problems.[3,18] Although the *in vitro* cellular spheroid model is often applied to study electrotransfection in a 3D context, these studies only focus on a single spheroid which fails to mimic the interactions between cells and the extracellular matrix.[19,20]

To date, the investigation of electroporation on 3D cultured cells and tissues has not been explored in the microfluidic platform yet. The benchtop method for electroporation study of 3D cells embedded in scaffolds showed very low transfection efficiency (~5%).[21] The major challenge is that the mass transport and mobility of delivered molecules in the cellular matrix are substantially restricted, and the migration becomes even more difficult when traveling into the cell spheroid.[22] Benchtop chemical transfection can handle scaffold embedded spheroid 3D cells. However, the protocols are tedious and lengthy, and require at least 24 hours of incubation.[23,24] Herein, we introduce a novel 3D microfluidic electrotransfection system (3D μ-electrotransfection) which provides facile, fast, and automated control for electrotransfection of 3D cultured cells. This 3D μ-electrotransfection system is simply fabricated by the 3D printing-assisted 3D molding and micro-assembling strategy, which employs the LEGO® concept to assemble a complicated 3D microchannel network as shown in Fig. 1a. Such a 3D perfusion microchannel network is unattainable by direct 3D printing or other microfabrication approaches, while it can facilitate the highly-efficient exchange of nutrition and waste for 3D cell growth. Multi-directional electric field scanning was achieved by employing four flat electrodes mounted into the 3D culture chamber *via* a 3D-printed holder and controlled by a programmable power sequencer (Fig. 1e and f). This multi-directional scanning not only can create transient pores all over the cell membrane, but also can generate local oscillation for enhancing mass transport and improving cell transfection efficiency.

As a proof-of-concept, we electro-delivered the pAcGFP1-C1 vector to 3D cultured HeLa cells in peptide hydrogel scaffolding for expressing GFP. The critical parameters were optimized including the electric field strength, plasmid concentration, pulse duration, and duty cycles. The 3D μ-electrotransfection system was further employed to genetically edit 3D cultured Hek-293 cells *via* delivery of CRISPR/Cas9 plasmid, which demonstrates the capability and holds the potential for future gene-editing based tissue repair, regenerative medicine, and gene therapy.

Experimental

3D printing and microfabrication of 3D μ-electrotransfection

3D structures were designed and drawn by SOLIDWORKS 2017. The resin mold containing the micro-structures was printed by a laptop-sized 3D printer (D3 ProJet 1200, 30 μm resolution) using VisiJet®FTX Clear resin (3D systems) for polydimethylsiloxane (PDMS) device production. The clear

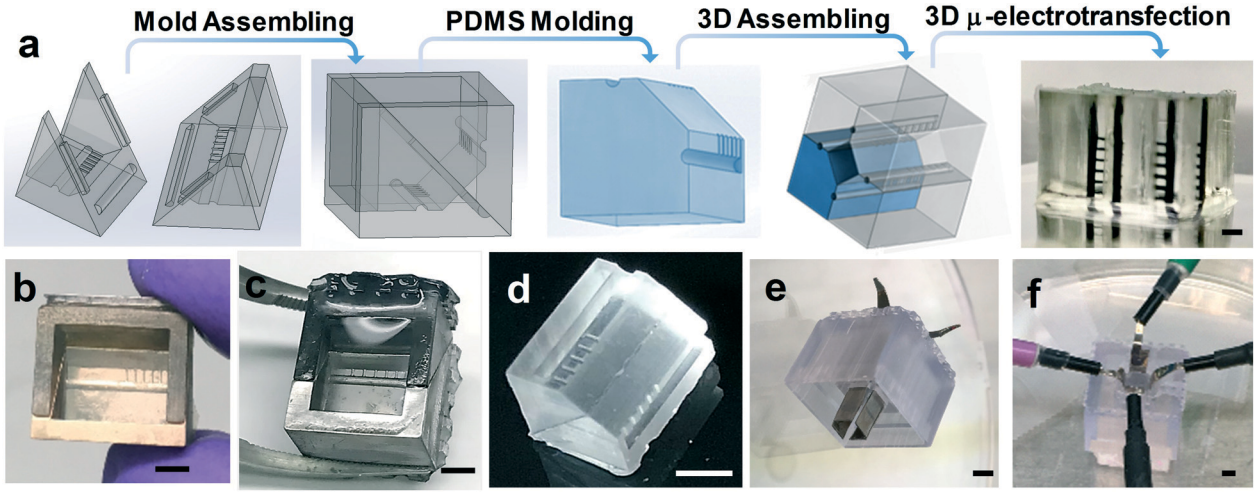

Fig. 1 3D printing assisted LEGO® assembly for building a 3D μ-electroporation system. a) The concept illustration of 3D printing, molding and LEGO® assembly. The last image shows the real four-piece assembled device bound to a glass slide with channels filled with black dye. The scale bar is 1 mm. b) 3D printed mold (2 pieces assembled) with the surface deposited with 20 nm Au. The scale bar is 2 mm. c) The mold (with 20 nm Ba coating) filled with PDMS and the molded PDMS part is shown in (d). The scale bar is 2 mm. e) Four electrodes mounted in a 3D printed holder. The scale bar is 2 mm. f) The setup of four electrodes on top of the cell culture chip for multi-dimensional electric frequency scanning. The electrodes are just fitting to the size of the culture chamber. The scale bar is 2 mm.

resin consists of triethylene glycol diacrylate, isobornyl methacrylate, and 2–3% photoinitiator phenylbis(2,4,6-trimethylbenzoyl)-phosphine oxide as described in the product information. The mold printing followed the reported protocols.[25,26] Freshly printed molds were cleaned using isopropyl alcohol under sonication, followed by 30 min post cure under UV light. A 20 nm thick palladium or gold coating was deposited onto the surface of the 3D-printed mold using a sputter coater (DENTON, DESK II). Prior to molding, the coated molds were conditioned with the surfactant solution (20% Tween20 in 80% isopropanol) for forming a dynamic micellar layer on the metal surface to facilitate the peel-off of polymer microstructures. PDMS was prepared using the standard 10 : 1 (base to curing agent) ratio. The PDMS mixture was degassed before being poured into the 3D-printed molds and then baked at 40 °C for 12 hours. The 3D printed molds are reusable after cleaning and conditioning. After the surface activation of molded PDMS pieces using a hand-held corona discharge treater (Electro-Technic Product, Chicago), the PDMS blocks were then assembled and bound as the 3D μ-electrotransfection device (Fig. 1). The assembly was conducted on a flat stage under a microscope (here we use the PDMS port creator stage, CorSolutions Inc.) which can guide the alignment easily. The assembled 3D μ-electrotransfection device was then bound to a glass slide to complete the fabrication.

3D cell culture and electro-transfection

HeLa cells (ATCC) and Hek-293 cells (ATCC) were cultured and maintained according to the ATCC standard protocol with Eagle's Minimum Essential Medium (EMEM, Sigma-Aldrich), supplemented with 10% (v/v) fetal bovine serum (FBS, Sigma-Aldrich), in a T-25 flask. The peptide hydrogel matrix (PepGel) was used as the scaffold with a peptide gel concentration of 0.2% for 3D cell culture. The 2D cells growing at a confluency of 80–90% were re-suspended with 0.25% trypsin/EDTA (Sigma-Aldrich) solution and centrifuged for 5 min at 250 *g*-force for seeding into the peptide hydrogel. The seeding density for 3D cell culture was $\sim 2.5 \times 10^5$ cells per mL. The 3D cell culture was carried out following a protocol described in the literature.[27] The medium exchange was performed from both the top of perfusion channels and the center cell culture chamber. From the top opening, we used a sharp pipette tip or syringe to suck out 2/3 of the old medium and inject the same amount of fresh medium.

A 4.7 kb plasmid pAcGFP1-C1 (Clontech, Mountain View) encoding green fluorescent protein (GFP) was amplified in NEB® 5-alpha Competent *E. coli* (New England Biolabs, Ipswich) and isolated using a QIAGEN Plasmid Maxi kit (QIAGEN GmbH). The plasmid purity was determined using a Nanodrop 2000 spectrophotometer. A 9.2 kb CRISPR/Cas9 vector pSpCas9(BB)-2A-GFP (PX458) (Addgene, MA) was amplified and purified following the same protocols as the preparation of GFP plasmid. The 2D standard electroporation protocols (Neon® transfection system) were used for validation of the 3D μ-electrotransfection system. The successfully transfected cells can express GFP as the reporter and be analyzed under flow cytometry (BD FACSAria IIIu, BD Biosciences) and confocal microscopy (Olympus IX81/3I spinning disk confocal inverted microscope).

3D COMSOL simulation

The AC/DC module was applied to simulate the electric field distribution in the 3D μ-electrotransfection system using the COMSOL Multiphysics software package (COMSOL Multiphysics 5.2). The equation governing electrostatics was numerically solved for the device to arrive at steady-state solutions. At steady state, the electric currents in a conductive medium are given by Ohm's law, which states

$$J = \sigma E + J_e$$

where σ is the electrical conductivity, J is the current density and E is the electric field. The electric field distribution was visualized using the below expression,

$$E = \mathrm{sqrt}(\mathrm{es.E}x \times \mathrm{es.E}x + \mathrm{es.E}y \times \mathrm{es.E}y + \mathrm{es.E}z \times \mathrm{es.E}z)$$

where es.Ex, es.Ey, and es.Ez are the components of the electric field in the dimension of x, y, and z, respectively. The conductivity of the electroporation buffer was set at 0.14 S m^{-1}.[28] The relative permittivity of the peptide hydrogel was set at 1 from the literature for a similar peptide hydrogel.[29] We carried out electrostatic numerical simulations to predict the distribution of electric field strength across the entire cell culture chamber. The multi-directional electric frequency scanning was simulated and performed following the protocol as shown in Fig. 2b. To simulate nutrient medium exchange and diffusion in the 3D μ-electrotransfection system, the transport of diluted species in a porous medium model was studied in a time-dependent manner. Three different cases, *i.e.* medium diffusion from the top medium to the cell matrix, medium diffusion from the side perfusion microchannel network to the cell matrix, and medium from both the top and the side perfusion microchannel network to the cell matrix, were investigated for comparison.

3D multi-directional electro-transfection

The voltage across the 3D cell culture chamber in multi-directional scanning was programmed and delivered by a HVS448 800 high voltage sequencer (LabSmith, CA, USA), which generated a square-wave electric pulse (see the ESI† video). Prior to applying the voltage, the cell medium (EMEM) was removed and 100 μL of low conductivity medium (Cytoporation® Medium T, BTX) was added to the top as well as the side perfusion channels. The electric potentials were applied to flat electrodes (Ag/Pa alloy, 3.5 mm width and 0.2 mm thick, Fisher). The electrodes were mounted using a customized holder, which was printed by a 3D printer

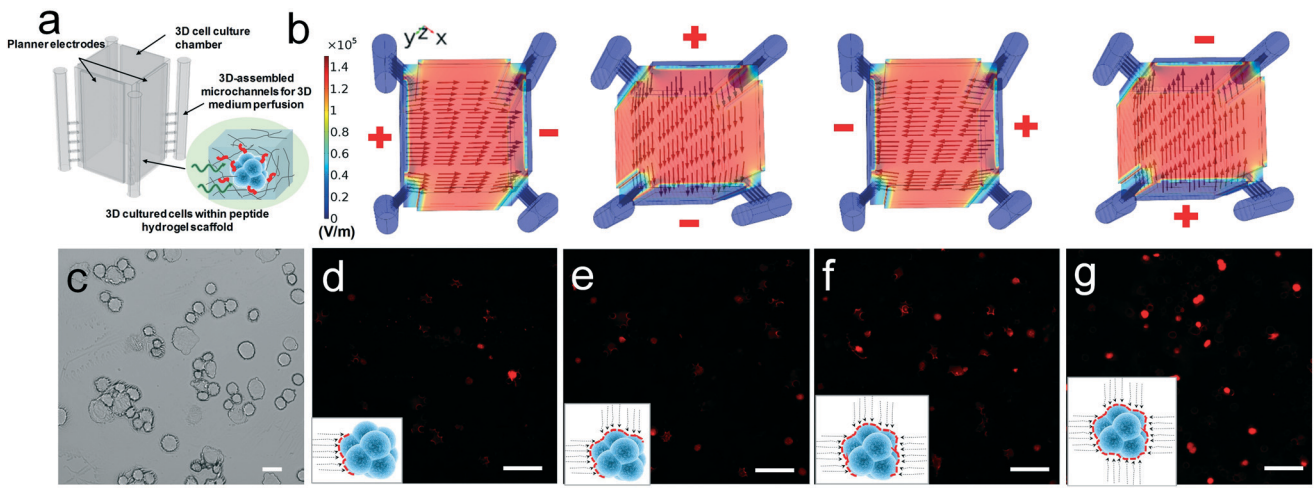

Fig. 2 a) Illustration of on-chip 3D cell culture. b) COMSOL simulation of the electric field distribution across the cell culture chamber with the multi-directional field scanning strategy. A voltage of 400 V was applied. Arrows indicate the intensity and direction of the electric field. c) Control sample without applying an electric field in bright field mode. The scale bar is 20 μm. d) One-direction electric field based PI delivery. e) Two-direction electric field based PI delivery. f) Three-direction electric field based PI delivery. g) Four-direction electric field based PI delivery. The scale bar is 50 μm for Fig. 2(d)–(g).

(D3 ProJet 1200) as shown in Fig. 1e. For transfection, the GFP plasmid was prepared in the gel matrix with cells to achieve a final concentration between 60 and 140 μg mL^{-1}. Cell culture was kept on ice during electroporation. Pulses at a frequency of 1 Hz were applied with a given electric field intensity. After electroporation, the low conductivity medium in cell culture was replaced by EMEM (pre-conditioned in 5% CO_2). The transfected 3D cells were cultured for two days and their GFP expression level was assessed by fluorescence microscopy and flow cytometry.

Investigation of cell membrane electro-permeabilization and propidium iodide delivery

3D cells were seeded on chip according to the previously described 3D culture method. After 24 hours of cell seeding, the culture medium was replaced by low conductivity medium and 20 μL of 10 μg mL^{-1} propidium iodide solution (PI, Sigma-Aldrich, USA) was added to the top of the cell culture. After 30 min of incubation, the electroporation was performed. To investigate the influence of the multi-directional electric field on the delivery of PI, four parallel experiments were conducted in terms of different electric field directions *i.e.* single direction, two cross directions, three directions and four directions (Fig. 2 and S1†). The total pulse duration was 32 ms for each experiment. The transfected cell cultures were transferred from chip to a 1.5 mL centrifuge tube. Without removing the upper layer cell medium, the gel was mechanically disrupted thoroughly by pipetting up and down. The mixture was centrifuged at 600*g* for 6 min. To break the colonies, 100 μL of Accumax™ solution (Sigma-Aldrich, USA) was added and incubated for 5 min at 37 °C. The results have been evaluated by cyto-spinning the cells on a glass slide followed by fluorescence microscopy analysis.

Flow cytometry analysis for assessing 3D electro-transfection efficiency and cell viability

The ready 3D transfected cultures were transferred from chip to a 1.5 mL centrifuge tube according to the method described in the PepGel protocol. The colonies were separated by Accumax™. To stain the dead cells, 5 μL of 10 μg mL^{-1} PI was added and incubated in the dark for 2 min. Thereafter, the mixture was centrifuged at 200*g* for 5 min and the cells were re-suspended with 200 μL PBS containing 0.5% BSA (w/v) for flow cytometry analysis. The transfection efficiency was evaluated based on flow cytometry to count the total number of GFP cells. The cell viability was evaluated based on flow cytometry counting of total dead cells. A total of 5000 events were measured in each sample at a flow rate of approximately 80 events per s.

Results and discussion

3D-printing enabled micro-assembly of the 3D μ-electrotransfection system

To build a 3D microfluidic electro-transfection system that is capable of uniform 3D electric field distribution as well as effective 3D cell culture, we conceived an electroporation chip as shown in Fig. 1. The conventional microfabrication approach is unable to construct such 3D microstructures, due to complicated protocols for accurate alignment and multi-layer bonding. In addition, it is very challenging to achieve direct 3D printing of monolithic 3D microstructures, particularly micro-scale hollow channels.[30,31] Therefore, we introduced the 3D-printing assisted molding of PDMS as LEGO® blocks for assembly into a more complicated 3D device. As illustrated in Fig. 1a, two designed parts were assembled as one transfer mold for PDMS molding. The assembled mold is detachable for easily releasing the PDMS parts. The PDMS

polymer was completely cured in the mold and no microstructural defects were identified during the demolding process (Fig. 1d). It is worth mentioning that high-temperature baking (*e.g.* >40 °C) should be avoided as the high temperature may cause physical structural distortion of the 3D printed resin. The molded PDMS polymer replicates microstructures as a single assembled unit as shown in Fig. 1c and d. After the assembly of four units with permanent bonding using surface plasma treatment, the 3D microfluidic electrotransfection device can be formed with four main vertical microchannels (~350 μm) each connected with five horizontal microchannels (~200 μm) (Fig. 1a). To facilitate the precise production of microstructures, a sputtered Ba or Au coating was deposited onto the mold surface in a thickness of 20 nm as shown in Fig. 1b and c. The final assembled device can be bound onto a glass slide after surface plasma treatment. The electrodes were fixed in a 3D printed holder (Fig. 1e), which fits the central culture chamber for electroporating 3D cultured cells (Fig. 1f and 2a).

Working principles of multi-directional electric field scanning enabled 3D transfection

In an electric field across cells, the cell membrane is an electric insulator that separates the extracellular medium from the intracellular medium. The ion concentration gradient between the outside and inside of the cellular membrane generates a resting potential difference, which is homogeneous across the cell membrane.[32] Upon application of voltage, such an electric potential difference across the cellular membrane will disrupt the field lines,[33,34] consequently, leading to the current being forced to flow around the cell and ionic layers being formed along the cellular membrane. The largest field line distortion is recognized at the sides of the membrane facing the field lines.[3,35] After reaching a certain intensity of field strength, the cell membrane can be disrupted to create transient pores. In a uniform electric field, the induced potential difference ($\Delta\psi$) at a point on the cell membrane and at a time after the rise of the electric pulse is given by:[3,36]

$$\Delta\psi = fg(\lambda)Er\cos(\theta)(1 - e^{-t/\tau_c})$$

where θ is the angle formed between the direction of the electric field and a normal point on the membrane. f is a factor related to the shape of the cell which is equal to 1.5 if the cell is spherical. $g(\gamma)$ is a factor related to the conductivity of the membrane. r is the semi-axis aligned along the electric field and τ_c is the charging time of the cell membrane. Because the membrane conductivity is extremely low compared to the conductivity of the intra and extracellular medium, it can be assumed that $g(\lambda) = 1$. As the electric field pulse duration (τ_c) is very small, at a steady state, considering the cell as a spherical insulator shell, $\Delta\Psi$ can be written in a simplified expression:

$$\Delta\psi = 1.5Er\cos(\theta)$$

Therefore, the induced potential difference on the cell membrane is directly proportional to the cell size and the strength of the electric field. Furthermore, the resting potential difference across the cell membrane reaches its maximum value at the side of the membrane facing the electric field directly (0° or 180°), while it decreases progressively along the cell surface up to the poles. Therefore, to open more pores on the cell membrane with mild voltage conditions, changing electric field directions to create pores from multiple sites on the cell membrane is more effective for electroporation. Therefore, in our experiments, the multi-directional electric frequency scanning method was developed, which can easily create transient pores all over the cell membrane along with the multi-directional scanning as demonstrated in Fig. 2b, as well as create local oscillation for enhancing mass transport and improving cell transfection efficiency. By COMSOL simulation in Fig. 2b, the uniform electric field strength across the cell chamber is estimated to be 1000 V cm^{-1} with a voltage of 500 V, which is sufficient to create transient pores on the cell membrane. In general, the electric field across cell clusters needs to reach the electroporation threshold (100 to 1000 V cm^{-1}, depending on the cell type) allowing membrane disruption.[3]

To prove the effectiveness of multi-directional electric field induced membrane permeabilization for delivering targets into the cytoplasm, a small molecule dye PI was electro-delivered in the 3D cell system. PI cannot enter living cells with an intact cell membrane, but can enter into the cytoplasm under electric field induced membrane permeabilization. Compared to other dyes with simultaneous permeation into living cells, the electro-delivery of PI can directly reflect the electric field induced membrane disruption and reseal process (electro-transfection). Note that our transfection voltage is 400 V (field strength is ~800 V cm^{-1}) with four electric pulses (16 ms) at a frequency of 1 Hz, which is kept the same for all the tests shown in Fig. 2d–g and S1,† but manipulated from different directions (illustrated in Fig. 2d–g insets). This electric field condition is below the literature reported, well-recognized electroporation field strength (~2000 V cm^{-1} for >80% cell viability) for HeLa cells.[37–39] Meanwhile, our experimental study showed that our voltage condition at 400 V can achieve more than 90% cell viability (Fig. 5a). Thus, we ascertain that the red staining of cells is due to the electro-transfection process, not the dead cells. The further illustration is shown in Fig. S1.† For clear visualization and evaluation of the amount of PI-delivered cells by our in-house inverted fluorescence microscope, we took the cells out of the hydrogel and dissociated cell clusters onto a glass slide for cytospinning and imaging. The fluorescence of cytospun cells on the glass slide was tracked by microscopy analysis to evaluate the PI delivery efficiency. The single direction of the electric field only showed ~40% cells transfected, which is much less than that with four directional scanning with over 80% cells transfected. Note that the total pulse duration for each test (d to g) was the same, so the adverse effects caused by the electric field

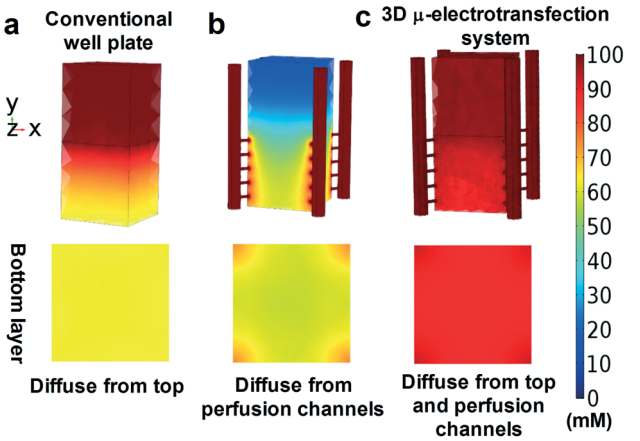

Fig. 3 COMSOL simulations of medium diffusion. a) Diffusion from the top medium to the cell matrix in the vertical direction for the conventional well plate. b) Diffusion from the microchannel network to the cell matrix in horizontal directions. c) Diffusion from both the microchannel network and top medium. 100 mM ionic strength was used in the fresh medium for simulation.

(heating, electrolysis, *etc.*) were comparable. The multi-directional scanning can cover the entire cell membrane for creating more transient pores. Additionally, compared to using one electric field direction with a long pulse duration, the short-duration pulsed scanning could reduce the risk of inducing irreversible electroporation, in turn, improving the cell viability.[40,41]

3D μ-electrotransfection system for 3D cell culture

Unlike the 3D cell culture in the well plate where the medium exchange only takes place from the top of well plates, our system allows multi-directional diffusion of the fresh medium from both the top of the cell matrix and the side of microchannel arrays surrounding the culture chamber in vertical and horizontal directions. In this culture system, diffusion is dominant and follows Fick's law. Assuming that the diffusion coefficient is the same for the three different configurations, the time of diffusion to reach the steady status is determined by the distance of the concentration gradient. The shorter travel distance leads to a shorter time, which in turn helps with better nutrient supply. Such a 3D perfusion microchannel network allows better nutrient support and waste exchange needed for the effective growth of 3D cells and tissues. Such diffusion-based perfusion has been well studied in 3D culture systems to include multiple perfusion channels, which is consistent with our design theory.[42,43] The growth rate is illustrated and calibrated in Fig. S2.† The cultured 3D cellular morphology is shown in Fig. S3† with a typical spheroid size of 100 μm (>10 cells). The mass transport and efficient diffusion of nutrients from multiple directions were proved by COMSOL simulation in Fig. 3, which indicates that the 3D perfusion microchannel network significantly improves the medium exchange compared to the conventional 3D cell culture in the well plate.

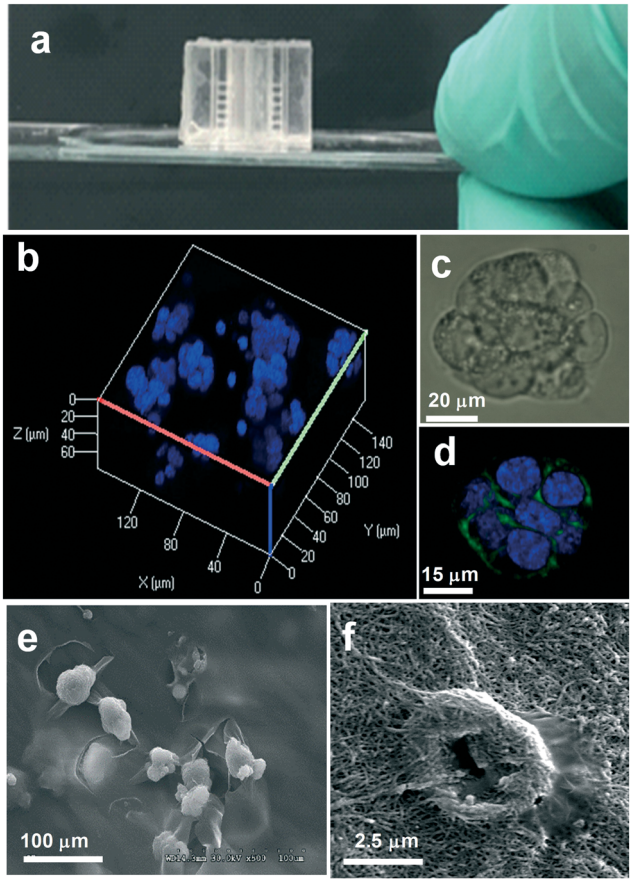

Fig. 4 On-chip 3D cell culture and microscopy characterization. a) Assembled PDMS chip bound to a glass slide for cell culture. b) Distribution of 3D-cultured HeLa cell spheroids in the peptide hydrogel under confocal microscope imaging. Nuclear DNA was stained with Hoechst. c) A close look at a single 3D cell spheroid in bright field mode and in the fluorescence channels in (d). The cell membrane was stained with FITC conjugated antibody–dye and the nuclear DNA was stained with Hoechst. e) SEM imaging of the cell spheroid distribution and the single spheroid interacting with peptide fibers in (f).

We chose the peptide hydrogel as the scaffold for 3D cell growth in our 3D μ-electrotransfection system shown in Fig. 4a, due to its high encapsulation stability, cell attachability and biocompatibility.[44,45] Upon crosslinking, the hydrogel forms a porous matrix with the pore size ranging from 200 to 400 nm, which gives a stable physical support for 3D cell growth as imaged in Fig. 4e and f.[27] Due to the perfusion microchannels for nutrient and waste exchange in our device, a high cell seeding density from 1×10^5 to 5×10^5 cells per mL can be achieved. The cell showed excellent attachability to peptide fibers (Fig. 4f). The dense spheroid distribution in the peptide hydrogel matrix in 3D as well as the morphology of a single spheroid has been characterized by confocal microscopy as shown in Fig. 4b–d. The confocal images depicting the different depths and locations of 3D cultured spheroids are shown in Fig. S4.† The side views demonstrated that cells are distributed along the height of the cell chamber. An individual 3D spheroid with a size of ~50 μm was observed after culturing for 4–5 days which is

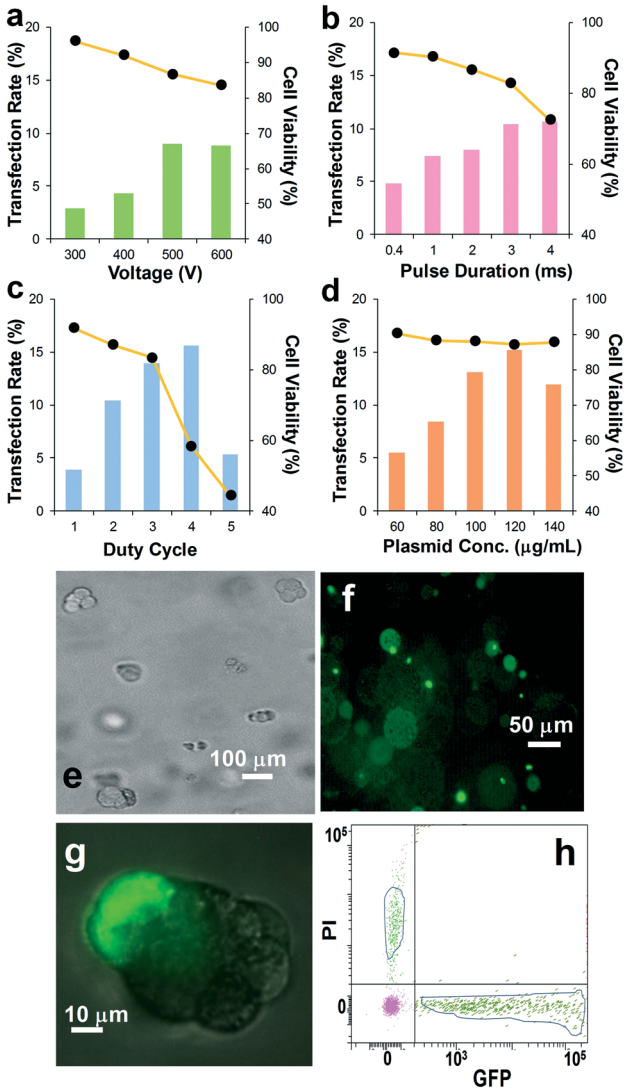

Fig. 5 Electro delivery of GFP plasmid to 3D cultured HeLa cell spheroids within the peptide hydrogel. a) Investigation of the influence of transfection voltage on the transfection rate and cell viability. The plasmid concentration is 100 μg mL^{-1}, the pulse duration is 2 ms, and the duty cycle is 2. b) Investigation of the influence of the pulse duration on the transfection rate and cell viability. The plasmid concentration is 100 μg mL^{-1}, the duty cycle is 2, and the transfection voltage is 500 V. c) Investigation of the influence of the duty cycle on the transfection rate and cell viability. The plasmid concentration is 100 μg mL^{-1}, the pulse duration is 3 ms, and the transfection voltage is 500 V. d) Investigation of the influence of the plasmid concentration on the transfection rate and cell viability. The pulse duration is 3 ms, the duty cycle is 3, and the transfection voltage is 500 V. The yellow dot lines in Fig. 5(a)–(d) indicate the cell viability. e) Electroporated sample in bright field mode and the FITC channel in (f). The transfection voltage was 500 V with a pulse duration of 3 ms for each direction, at a frequency of 1 Hz and 3 duty cycles. g) Confocal image of a transfected cell spheroid. h) Representative flow cytometry graph to evaluate the GFP positive cell and PI positive cell for estimating cell transfection efficiency and cell viability. The transfection voltage was 500 V with a pulse duration of 3 ms for each direction, at a frequency of 1 Hz and 3 duty cycles. The cell transfection efficiency is 13.5% with 85% cell viability.

composed of ~10 cells as shown in Fig. 4c and d. Such morphology characterization indicates that our 3D μ-electrotransfection system provides a suitable microenvironment for growing 3D cells and tissues, which is enabled by the implementation of 3D perfusion microchannels.

3D μ-electrotransfection of 3D cultured cells

To assess the transfection efficiency and cell viability of our 3D μ-electrotransfection system, a plasmid DNA (pAcGFP1-C1) encoding GFP was electroporated into 3D cultured HeLa cells. For conventional electrotransfection of the 2D cell suspension, the critical electric field needs to reach a value in the range from 100 to 1000 V cm^{-1} (depending on cell size and electric field properties) to disrupt the cell membrane and ensure reversible electroporation.[3,46] In the case of spheroid cells, the low electric field (~500 V cm^{-1}) with long pulses (~20 ms) has been reported which leads to transfected GFP expression.[19,47] In contrast to the study of cell suspensions or isolated cell spheroids, we intended to deliver plasmid directly to 3D cells embedded in the extracellular matrix to mimic electroporation of an *in vivo*-like tissue microenvironment. Thus, we optimized the key parameters that control the electroporation efficiency, including the electric field strength, plasmid concentration, pulse duration, and duty cycles.

Experiments were carried out after the cells were seeded on the chip for 48 hours. Fig. 5e–h show a typical image and flow cytometry analysis of 3D cultured cells after electrotransfection in our system. The confocal microscopy imaging in Fig. 5e–g displays a transfected 3D cell spheroid with a diameter around 60 μm. With a voltage of 300 V in multi-directional field scanning (equal to an electric field of 750 V cm^{-1}), 2.5% GFP expressed cells were identified from the total cell population with a cell viability of ~95% by flow cytometry analysis (Fig. 5). The transfection efficiency increased with increasing the applied voltage from 300 V to 600 V. However, the cell viability was decreased from ~96% to ~84%, due to more dead cells caused by the high voltage, which in turn decreases the transfection efficiency with a higher voltage of 600 V (1500 V cm^{-1}) (Fig. 5a–d). Either increasing the pulse duration or adding more duty cycles can lead to an increase of transfection efficiency, but the dead cells were dramatically increased accordingly, due to the irreversible harsh electric interruption of the cell membrane. Applying 4 duty cycles led to 15.6% transfection efficiency but with 58.3% cell viability. To find the balance between the transfection efficiency and cell viability for the best transfection outcome, the optimized voltage is 500 V with ~120 μg mL^{-1} plasmid concentration, which showed a more important role in the control of good cell viability compared to the electric duty cycle and pulse. Increasing the plasmid concentration will create more contact opportunities between cells and plasmids, reflecting an increasing number of transfected cells. We kept the pulse duration of 3 ms, 3 duty cycles and transfection voltage of 500 V. Using the optimal plasmid concentration of

~120 μg mL^{-1}, we achieved 15.2% transfection efficiency with 87.1% cell viability, which is 3-fold higher than that of the currently reported benchtop 3D electro-transfection method[21] with better cell viability. However, continuously increasing the plasmid DNA concentration did not result in higher transfection efficiency. This observation agrees with the previous report that there is a maximum plasmid concentration for gene delivery.[48] Compared to 2D cell transfection, the optimal plasmid concentration for 3D cell electroporation is much higher (110 *vs.* 40 μg mL^{-1}).[49] This is attributed to the porous peptide hydrogel matrix which limits the travel of plasmid to cells and requires a higher amount of plasmid to enhance contact opportunities with cells. In addition to the scaffold matrix effect, the 3D cell spheroid is much bigger than an individual cell and the plasmid needs to travel a long distance to reach the cells inside the cluster, which makes gene delivery difficult. Our method with the electric field scanning strategy could improve mass transport to address this challenge.

The Hek-293 cells are the classic model cell line for studying electro-delivery of CRISPR/Cas9.[50,51] For proving the applicability of our system in 3D tissue engineering, we transfected the CRISPR/Cas9 gene with 3D cultured Hek-293 cells. CRISPR/Cas9 editing has emerged as a rapid and powerful approach to make precise and targeted changes in the genome of living cells.[52] Recent studies have successfully demonstrated gene transfer to organoids using various methods including lentivirus transfection,[53] liposomal transfection[54] and electroporation.[55] The advantage of electroporation over other methods is that it avoids the use of harmful chemicals in the culture system. The plasmid can be delivered upon preparation and does not require the production of lentivirus or carriers, which significantly reduces labor and time. In this experiment, a 9.2 kb PX458 vector was delivered to 3D cultured Hek-293 cells using our 3D μ-electrotransfection system. The EGFP protein encoded by this CRISPR/Cas9 vector was traced to evaluate the CRISPR/Cas9 delivery. A high concentration of CRISPR/Cas9 plasmid (200 μg mL^{-1}) was applied according to previously optimized conditions, and a mild voltage (400 V) and 2 duty cycles were chosen. Fig. 6a shows the 3D distribution of transfected Hek cells within the cultured extracellular matrix (1.5 mm × 1 mm × 0.5 mm). This image is a Multi-Stack Montage of the *x*-scan, *y*-scan and *z*-scan on a large scale. Thus, each GFP expressed 3D cell cluster is viewed as a green dot. Fluorescence confocal imaging was performed with the 3D gel matrix which introduced the background shown as red, due to light diffraction from the dense mesh gel structure. Fig. 6b shows the successfully transfected cell spheroids with ~25 cells in a perfect round cluster. Fig. 6c shows a single transfected cell in the status of division. The uniform green fluorescence distribution within either the spheroid cluster or the divided two daughter cells proves the effective electroporation across the cell cytoplasm. We also performed nucleus staining using DAPI as shown in Fig. 6f and g which clearly showed the multiple cells clustered together to form this sphere shape. The clearance of the peptide hydrogel scaffold background is very critical in confocal imaging. We summarized the protocols developed in our lab in the ESI.† We also used the confocal imaging analysis tool "spot annotation" to count the number of cell nuclei across the *Z* stack in the region of interest. We measured multiple spheroids, and the average cell number is ~25. We also measured the typical cluster size using confocal imaging analysis and the average spheroid size is about ~75–100 μm which is clustered by ~25–50 individual cells. We further tuned the parameters by varying the electric field strength and pulse duration; however, the transfection efficiency is not significantly improved. It is speculated that due to the bigger size of the CRISPR gene, it may not freely transport within the porous scaffold or enter the cell transient pores. It is also likely that

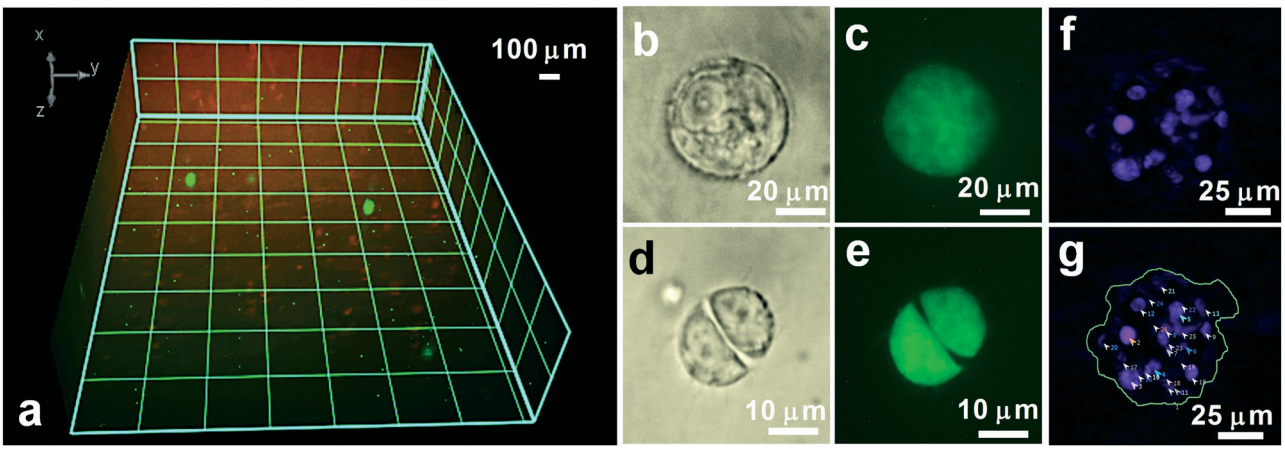

Fig. 6 Electroporating the CRISPR/Cas9 plasmid (PX458) to 3D cultured Hek-293 cells. a) The overview of the transfected cells in the 3D matrix (1.5 mm × 1 mm × 0.5 mm). This image is from the stacking of the *x*-scan, *y*-scan and *z*-scan (Multi Stack Montage) on a large scale. Thus, each GFP expressed 3D cell cluster is viewed as a green dot. b) A transfected Hek-293 cell spheroid (~25 cells) in bright field mode and in the FITC channel in (c). d) A single transfected cell in the status of division in bright field mode and the FITC channel in (e). f) Confocal image showing the DAPI stained cell nuclei which proved that multiple individual cells form the perfect 3D round shape of the Hek spheroid. g) Confocal imaging analysis of the cell nuclei across the *Z* stack using spot annotation to the region of interest.

the gene editing efficiency[56–58] may not represent the transfection efficiency due to off-target expression. Note that in these experiments we used the green fluorescence emitted from GFP expressed cells to evaluate this transfection process. We could use a selective medium to remove non-transfected cells for continuously culturing CRISPR gene edited 3D cells for achieving the regulation of tissue functions.

Conclusions

In recent years, 3D printing has been drawing much attention from the research community, and can create complex structures with high quality for fast prototyping,[59–61] compared to the traditional micro-fabrication. As a layer-by-layer manufacturing method, 3D printing not only achieves monolithic device fabrication but also allows for printing molds in producing PDMS microfluidic chips. However, constructing complex 3D structures and monolithic hollow channels on the micro-scale is still challenging. In this paper, we take advantage of 3D printing and the LEGO® assembly concept for re-constructing more complicated 3D microfluidic channels, which extends the 3D printing capability for creating unattainable 3D micro-geometries and introducing geometrics enabled functionality. Such an assembled 3D μ-electrotransfection system allows spatial and temporal control of the electric field uniformly in three dimensions. Therefore, multi-directional electric frequency scanning is achievable for maximizing the electroporation efficiency *via* enhancing the resting potential difference across the cell membrane. Furthermore, this scanning process also creates local oscillation for enhancing mass transport and improving cell transfection efficiency.[62] The 3D-cell culture performance is improved as well due to the enhanced medium perfusion *via* inter-connected vertical and horizontal perfusion microchannel arrays, which are reconstructed by this 3D printing-assisted molding and assembly process.

Existing microfluidic electroporation approaches are only able to study monolayer cell suspensions *in vitro*, and are incapable of clinical translation within an *in vivo* tissue microenvironment, but essential in gene therapy and tissue repair. Up to now, the study of electroporation on 3D cultured cells within the extracellular matrix has not been well explored. Thus, our work could build an effective 3D-cell electroporation model to bridge such a gap. Our work introduced the first 3D microfluidic electroporation system for transfecting 3D cultured cells, which demonstrated a ~3-fold increase in transfection efficiency with good cell viability (>85%), compared to the conventional benchtop 3D-cell electro-transfection.[21] The optimization of several key parameters, including the electric field strength, plasmid concentration, pulse duration and duty cycles, gave a good rationale for understanding the influence on the delivery process and cell viability. The threshold of permeabilization voltage and plasmid concentration play more important roles, due to the direct connection with the chances of transient pore opening and contact. Due to the limited mass transport of cargos through the porous cellular matrix to cells, the 3D transfection is more challenging. The hard-to-transfect cells generally have lower transfection efficiency. Our approach with the multi-dimensional frequency scanning enhanced the transfection efficiency, compared to currently existing 3D electroporation methods.[21] Compared with other transfection approaches, such as the chemical transfection of scaffold embedded 3D cells which requires more than 24 hours of incubation, our approach is much simpler and faster (less than 1 hour).

The HeLa and Hek-293 cells are classic model cell lines for studying electroporation, due to their biological stability during culture growth. Thus, this study could serve as a good cross reference for demonstrating the performance of our device in terms of 3D culture and 3D electroporation. The voltage threshold for cellular electroporation and opening transient pores is cell-type dependent.[3] Generally, no matter what type of transfection approach, 3D spheroids that are composed of 3D cells are more difficult to transfect compared to floating individual cells, due to the irregular and dense 3D cellular morphology, as well as the complicated scaffold materials. Our 3D culture method grows single individual cells into 3D spheroids in the scaffold, which mimic the *in vivo* cellular interactions with the ECM. The typical size of spheroids is around ~50–150 μm (~10 cells per spheroid), which is consistent with other reported 3D culture methods.[27,63–65]

This study can also mimic the intracellular delivery of therapeutic molecules *in vivo* and has important implications for gene delivery in tissues, especially for editing cells *in vivo* using the CRISPR/Cas9 method. Future work will be conducted to further enhance transfection efficiency by investigating different scaffolds with various conductivities and porosities. This 3D reconstructed μ-electrotransfection platform can serve as a good model system for studying and mimicking the *in vivo* electrotransfection process, and building the foundation for developing more effective clinical gene delivery approaches.

Conflicts of interest

There are no conflicts to declare.

Acknowledgements

We acknowledge the funding support from USDA-NIFA KS451214 and NIH P20 NIH0078730, as well as the K-INBRE Postdoctoral Scholarship (P20 GM103418) for QZ. We also acknowledge the assistance from the Confocal Core at the University of Kansas and the Kansas State University for imaging 3D cells.

References

1 M. P. Stewart, A. Sharei, X. Ding, G. Sahay, R. Langer and K. F. Jensen, In vitro and ex vivo strategies for intracellular delivery, *Nature*, 2016, **538**, 183.
2 C. H. Evans and J. Huard, Gene therapy approaches to regenerating the musculoskeletal system, *Nat. Rev. Rheumatol.*, 2015, **11**, 234.

3 R. Christelle, M. Sasa Haberl, Z. Andreas, R. Marie-Pierre and M. Damijan, Gene Electrotransfer: A Mechanistic Perspective, *Curr. Gene Ther.*, 2016, **16**(2), 98–129.
4 J. A. Impellizeri, G. Ciliberto and L. Aurisicchio, Electrogene-transfer as a new tool for cancer immunotherapy in animals, *Vet. Comp. Oncol.*, 2014, **12**(4), 310–318.
5 K. E. Broderick and L. M. Humeau, Electroporation-enhanced delivery of nucleic acid vaccines, *Expert Rev. Vaccines*, 2015, **14**(2), 195–204.
6 N. Bhattacharjee, L. F. Horowitz and A. Folch, Continuous-flow multi-pulse electroporation at low DC voltages by microfluidic flipping of the voltage space topology, *Appl. Phys. Lett.*, 2016, **109**(16), 163702.
7 P. A. Garcia, Z. Ge, J. L. Moran and C. R. Buie, Microfluidic Screening of Electric Fields for Electroporation, *Sci. Rep.*, 2016, **6**, 21238.
8 S. Bian, Y. Zhou, Y. Hu, J. Cheng, X. Chen, Y. Xu and P. Liu, High-throughput in situ cell electroporation microsystem for parallel delivery of single guide RNAs into mammalian cells, *Sci. Rep.*, 2017, **7**, 42512.
9 T. Geng and C. Lu, Microfluidic electroporation for cellular analysis and delivery, *Lab Chip*, 2013, **13**(19), 3803–3821.
10 H. Yun and S. C. Hur, Sequential multi-molecule delivery using vortex-assisted electroporation, *Lab Chip*, 2013, **13**(14), 2764–2772.
11 L. Chang, L. Li, J. Shi, Y. Sheng, W. Lu, D. Gallego-Perez and L. J. Lee, Micro-/nanoscale electroporation, *Lab Chip*, 2016, **16**(21), 4047–4062.
12 M. B. Fox, D. C. Esveld, A. Valero, R. Luttge, H. C. Mastwijk, P. V. Bartels, A. van den Berg and R. M. Boom, Electroporation of cells in microfluidic devices: a review, *Anal. Bioanal. Chem.*, 2006, **385**(3), 474–485.
13 H. Lu, M. A. Schmidt and K. F. Jensen, A microfluidic electroporation device for cell lysis, *Lab Chip*, 2005, **5**(1), 23–29.
14 M. Ravi, V. Paramesh, S. R. Kaviya, E. Anuradha and F. D. Solomon, 3D cell culture systems: advantages and applications, *J. Cell. Physiol.*, 2015, **230**(1), 16–26.
15 B. A. Justice, N. A. Badr and R. A. Felder, 3D cell culture opens new dimensions in cell-based assays, *Drug Discovery Today*, 2009, **14**(1), 102–107.
16 M. Kandušer and D. Miklavčič, *Electroporation in Biological Cell and Tissue: An Overview. In Electrotechnologies for Extraction from Food Plants and Biomaterials*, Springer New York, New York, NY, 2008, pp. 1–37.
17 M. P. Stewart, R. Langer and K. F. Jensen, Intracellular Delivery by Membrane Disruption: Mechanisms, Strategies, and Concepts, *Chem. Rev.*, 2018, **118**(16), 7409–7531.
18 Y. Zhang, A. Satterlee and L. Huang, In vivo gene delivery by nonviral vectors: overcoming hurdles?, *Mol. Ther.*, 2012, **20**(7), 1298–1304.
19 L. Wasungu, J. M. Escoffre, A. Valette, J. Teissie and M. P. Rols, A 3D in vitro spheroid model as a way to study the mechanisms of electroporation, *Int. J. Pharm.*, 2009, **379**(2), 278–284.
20 L. Gibot and M. P. Rols, 3D spheroids' sensitivity to electric field pulses depends on their size, *J. Membr. Biol.*, 2013, **246**(10), 745–750.
21 S. Haberl and M. Pavlin, Use of collagen gel as a three-dimensional in vitro model to study electropermeabilization and gene electrotransfer, *J. Membr. Biol.*, 2010, **236**(1), 87–95.
22 L. Gibot and M.-P. Rols, 3D Spheroids' Sensitivity to Electric Field Pulses Depends on Their Size, *J. Membr. Biol.*, 2013, **246**(10), 745–750.
23 C. Sapet, C. Formosa, F. Sicard, E. Bertosio, O. Zelphati and N. Laurent, 3D-fection: cell transfection within 3D scaffolds and hydrogels, *Ther. Delivery*, 2013, **4**(6), 673–685.
24 R. G. Morgan, A. C. Chambers, D. N. Legge, S. J. Coles, A. Greenhough and A. C. Williams, Optimized delivery of siRNA into 3D tumor spheroid cultures in situ, *Sci. Rep.*, 2018, **8**(1), 7952.
25 K. Plevniak, M. Campbell, T. Myers, A. Hodges and M. He, 3D printed auto-mixing chip enables rapid smartphone diagnosis of anemia, *Biomicrofluidics*, 2016, **10**(5), 054113.
26 Q. Zhu, Z. Zhu and M. He, *3D Additive Manufacturing and Micro-Assembly for Transfection of 3D-Cultured Cells and Tissues. Conference: ASME 2018 13th International Manufacturing Science and Engineering Conference*, 2018.
27 H. Huang, Y. Ding, X. S. Sun and T. A. Nguyen, Peptide Hydrogelation and Cell Encapsulation for 3D Culture of MCF-7 Breast Cancer Cells, *PLoS One*, 2013, **8**(3), e59482.
28 T. Geng, Y. Zhan, J. Wang and C. Lu, Transfection of cells using flow-through electroporation based on constant voltage, *Nat. Protoc.*, 2011, **6**(8), 1192–1208.
29 N. Ashwanikumar, N. A. Kumar, P. S. Saneesh Babu, K. C. Sivakumar, M. V. Vadakkan, P. Nair, I. Hema Saranya, S. Asha Nair and G. S. Vinod Kumar, Self-assembling peptide nanofibers containing phenylalanine for the controlled release of 5-fluorouracil, *Int. J. Nanomed.*, 2016, **11**, 5583–5594.
30 S. Waheed, J. M. Cabot, N. P. Macdonald, T. Lewis, R. M. Guijt, B. Paull and M. C. Breadmore, 3D printed microfluidic devices: enablers and barriers, *Lab Chip*, 2016, **16**(11), 1993–2013.
31 R. D. Sochol, E. Sweet, C. C. Glick, S.-Y. Wu, C. Yang, M. Restaino and L. Lin, 3D printed microfluidics and microelectronics, *Microelectron. Eng.*, 2018, **189**, 52–68.
32 P. T. Gaynor and P. S. Bodger, Physical modelling of electroporation in close cell-to-cell proximity environments, *Phys. Med. Biol.*, 2006, **51**(12), 3175–3188.
33 F. André and L. M. Mir, DNA electrotransfer: its principles and an updated review of its therapeutic applications, *Gene Ther.*, 2004, **11**, S33.
34 U. Zimmermann, Electric field-mediated fusion and related electrical phenomena, *Biochim. Biophys. Acta, Biomembr.*, 1982, **694**(3), 227–277.
35 W. Krassowska and P. D. Filev, Modeling Electroporation in a Single Cell, *Biophys. J.*, 2007, **92**(2), 404–417.
36 J. Teissie and M. P. Rols, An Experimental Evaluation of the Critical Potential Difference Inducing Cell-Membrane Electropermeabilization, *Biophys. J.*, 1993, **65**(1), 409–413.

37 L. Chicaybam, C. Barcelos, B. Peixoto, M. Carneiro, C. G. Limia, P. Redondo, C. Lira, F. Paraguassu-Braga, Z. F. Vasconcelos, L. Barros and M. H. Bonamino, An Efficient Electroporation Protocol for the Genetic Modification of Mammalian Cells, *Front. Bioeng. Biotechnol.*, 2016, **4**, 99.

38 B. D. Hornstein, D. Roman, L. M. Arevalo-Soliz, M. A. Engevik and L. Zechiedrich, Effects of Circular DNA Length on Transfection Efficiency by Electroporation into HeLa Cells, *PLoS One*, 2016, **11**(12), e0167537.

39 J. Glahder, B. Norrild, M. B. Persson and B. R. Persson, Transfection of HeLa-cells with pEGFP plasmid by impedance power-assisted electroporation, *Biotechnol. Bioeng.*, 2005, **92**(3), 267–276.

40 C. Sun, Z. Cao, M. Wu and C. Lu, Intracellular Tracking of Single Native Molecules with Electroporation-Delivered Quantum Dots, *Anal. Chem.*, 2014, **86**(22), 11403–11409.

41 Y. Zhan, Z. Cao, N. Bao, J. Li, J. Wang, T. Geng, H. Lin and C. Lu, Low-frequency ac electroporation shows strong frequency dependence and yields comparable transfection results to dc electroporation, *J. Controlled Release*, 2012, **160**(3), 570–576.

42 M. Piola, M. Soncini, M. Cantini, N. Sadr, G. Ferrario and G. B. Fiore, Design and functional testing of a multichamber perfusion platform for three-dimensional scaffolds, *Sci. World J.*, 2013, **2013**, 123974.

43 J. Rouwkema, B. Koopman, C. Blitterswijk, W. Dhert and J. Malda, Supply of nutrients to cells in engineered tissues, *Biotechnol. Genet. Eng. Rev.*, 2010, **26**, 163–178.

44 Y. Zhiqiang, X. Quan, D. Chenbo, L. Su Seong, G. Liqian, L. Yiwen, D. Mathew and W. Ortenzio; Jun, Self-Assembling Peptide Nanofibrous Hydrogel as a Versatile Drug Delivery Platform, *Curr. Pharm. Des.*, 2015, **21**(29), 4342–4354.

45 A. M. Jonker, D. W. P. M. Löwik and J. C. M. van Hest, Peptide- and Protein-Based Hydrogels, *Chem. Mater.*, 2012, **24**(5), 759–773.

46 P. A. Garcia, Z. Ge, J. L. Moran and C. R. Buie, Microfluidic Screening of Electric Fields for Electroporation, *Sci. Rep.*, 2016, **6**, 21238.

47 B. Marrero and R. Heller, The use of an in vitro 3D melanoma model to predict in vivo plasmid transfection using electroporation, *Biomaterials*, 2012, **33**(10), 3036–3046.

48 H. Potter, Transfection by Electroporation, *Curr. Protoc. Mol. Biol.*, 2003, 1–12, Chapter: Unit-9.3.

49 M. Tatsufumi and S. Yoshihide, Plasmid DNA Gene Therapy by Electroporation: Principles and Recent Advances, *Curr. Gene Ther.*, 2011, **11**(6), 447–456.

50 C. A. Lino, J. C. Harper, J. P. Carney and J. A. Timlin, Delivering CRISPR: a review of the challenges and approaches, *Drug Delivery*, 2018, **25**(1), 1234–1257.

51 Z. Li, J. Zhao, N. Muhammad, D. Wang, Q. Mao and H. Xia, Establishment of a HEK293 cell line by CRISPR/Cas9-mediated luciferase knock-in to study transcriptional regulation of the human SREBP1 gene, *Biotechnol. Lett.*, 2018, **40**(11–12), 1495–1506.

52 F. A. Ran, P. D. Hsu, J. Wright, V. Agarwala, D. A. Scott and F. Zhang, Genome engineering using the CRISPR-Cas9 system, *Nat. Protoc.*, 2013, **8**(11), 2281–2308.

53 B.-K. Koo, D. E. Stange, T. Sato, W. Karthaus, H. F. Farin, M. Huch, J. H. van Es and H. Clevers, Controlled gene expression in primary Lgr5 organoid cultures, *Nat. Methods*, 2011, **9**, 81.

54 G. Schwank, B.-K. Koo, V. Sasselli, J. F. Dekkers, I. Heo, T. Demircan, N. Sasaki, S. Boymans, E. Cuppen, C. K. van der Ent, E. E. S. Nieuwenhuis, J. M. Beekman and H. Clevers, Functional Repair of CFTR by CRISPR/Cas9 in Intestinal Stem Cell Organoids of Cystic Fibrosis Patients, *Cell Stem Cell*, 2013, **13**(6), 653–658.

55 M. Fujii, M. Matano, K. Nanki and T. Sato, Efficient genetic engineering of human intestinal organoids using electroporation, *Nat. Protoc.*, 2015, **10**, 1474.

56 X. Wang, J. Lu, K. Lao, S. Wang, X. Mo, X. Xu, X. Chen and B. Mo, Increasing the efficiency of CRISPR/Cas9-based gene editing by suppressing RNAi in plants, *Sci. China: Life Sci.*, 2019, 1–3.

57 Y. Mao, X. Yang, Y. Zhou, Z. Zhang, J. R. Botella and J. K. Zhu, Manipulating plant RNA-silencing pathways to improve the gene editing efficiency of CRISPR/Cas9 systems, *Genome Biol.*, 2018, **19**(1), 149.

58 V. T. Chu, T. Weber, B. Wefers, W. Wurst, S. Sander, K. Rajewsky and R. Kuhn, Increasing the efficiency of homology-directed repair for CRISPR-Cas9-induced precise gene editing in mammalian cells, *Nat. Biotechnol.*, 2015, **33**(5), 543–548.

59 N. Bhattacharjee, A. Urrios, S. Kang and A. Folch, The upcoming 3D-printing revolution in microfluidics, *Lab Chip*, 2016, **16**(10), 1720–1742.

60 S. Waheed, J. M. Cabot, N. P. Macdonald, T. Lewis, R. M. Guijt, B. Paull and M. C. Breadmore, 3D printed microfluidic devices: enablers and barriers, *Lab Chip*, 2016, **16**(11), 1993–2013.

61 H. Yong, W. Yan, F. Jian-zhong, G. Qing and Q. Jing-jiang, Developments of 3D Printing Microfluidics and Applications in Chemistry and Biology: a Review, *Electroanalysis*, 2016, **28**(8), 1658–1678.

62 M. Rebersek, C. Faurie, M. Kanduser, S. Corovic, J. Teissie, M. P. Rols and D. Miklavcic, Electroporator with automatic change of electric field direction improves gene electrotransfer in-vitro, *J. Geophys. Res. Planets*, 2007, **6**, 25.

63 G. Y. Lee, P. A. Kenny, E. H. Lee and M. J. Bissell, Three-dimensional culture models of normal and malignant breast epithelial cells, *Nat. Methods*, 2007, **4**, 359.

64 M. Wolun-Cholewa, K. Langer, K. Szymanowski, A. Glodek, A. Jankowska, W. Warchol and J. Langer, An Efficient 3D Cell Culture Method on Biomimetic Nanostructured Grids, *PLoS One*, 2013, **8**(9), e72936.

65 M. W. Tibbitt and K. S. Anseth, Hydrogels as extracellular matrix mimics for 3D cell culture, *Biotechnol. Bioeng.*, 2009, **103**(4), 655–663.

